

TAE-YEONG SO¹, NAM-SEOK KIM¹, YOUNG-CHUL SHIN^{1*}, CHANG-HEE CHO²

EFFECT OF TEMPERATURE ON MICROSTRUCTURE AND TEXTURE DEVELOPMENT IN A7075 ALUMINUM ALLOY SUBJECTED TO BIAXIAL ALTERNATE FORGING

In this study, the microstructural evolution of an A7075 aluminum alloy subjected to severe deformation by biaxial alternate forging (BAF) was investigated at room temperature (RT) and 300°C. SEM-BSE observations revealed no significant differences in the morphology or distribution of second-phase particles between the two conditions, indicating that deformation temperature did not markedly affect particle fragmentation at the applied strain level. However, SEM-EDS analysis of the matrix showed a noticeable reduction in Zn content after deformation at 300°C compared to RT, suggesting enhanced solute redistribution during high-temperature deformation. EBSD analyses demonstrated clear differences in deformation microstructures depending on both temperature and strain localization. At RT, the high-deformation region exhibited pronounced lattice distortion and heterogeneous orientation gradients, whereas deformation at 300°C resulted in more uniform IQ contrast and reduced intragranular misorientation, indicative of active recovery. Texture analysis based on ODF sections and pole figures showed moderate development of shear and rolling texture components, with more continuous and stabilized texture features at 300°C. These results indicate that elevated-temperature BAF promotes solute redistribution and recovery-assisted plastic flow without significant alteration of second-phase characteristics.

Keywords: A7075 aluminum alloy; Biaxial alternate forging; Severe plastic deformation; Texture evolution

1. Introduction

A7075 aluminum alloy, belonging to the Al–Zn–Mg–Cu system, is widely used in aerospace and transportation applications due to its excellent strength-to-weight ratio achieved through precipitation strengthening. However, the high strength of A7075 is accompanied by limited ductility and poor workability, making severe plastic deformation and forming processes particularly challenging at room temperature. As a result, elevated-temperature deformation is often employed to improve formability by activating diffusion-assisted mechanisms such as recovery and solute redistribution, while retaining the alloy's high-strength potential [1-3].

Biaxial alternate forging (BAF) is a severe plastic deformation technique that introduces large cumulative strain into bulk materials through repeated forging along orthogonal directions while maintaining specimen geometry [4-7]. Previous studies have demonstrated that BAF can be successfully applied to various aluminum alloys, including Al–Mg and Al–Mg–Si systems, enabling the accumulation of high effective strain even at room

temperature. The deformation during BAF is primarily accommodated by intensive dislocation multiplication, slip band development, and localized strain partitioning, rather than by dynamic recrystallization. Owing to its ability to impose both concentrated and distributed deformation, BAF has been shown to be effective for evaluating forgeability limits and deformation stability of difficult-to-form aluminum alloys. These studies collectively indicate that BAF provides a useful experimental framework for investigating temperature-dependent deformation mechanisms and microstructural evolution in high-strength aluminum alloys.

Accordingly, in this study, BAF was applied to the high-strength and poor-workability A7075 aluminum alloy to examine its deformation behavior under severe plastic deformation conditions. Despite the extensive use of BAF for Al–Mg-based alloys, the formation of deformation microstructures in precipitation-hardened Al–Zn–Mg–Cu alloys such as A7075 has not been sufficiently explored. The objective of this work is to characterize the microstructural evolution induced by BAF in A7075 alloy, with particular emphasis on deformation-induced changes in the matrix state under elevated-temperature deformation.

¹ KOREA INSTITUTE OF INDUSTRIAL TECHNOLOGY (KITECH), INCHEON 21999, REPUBLIC OF KOREA

² NORTHWESTERN UNIVERSITY DEPARTMENT OF MATERIALS SCIENCE AND ENGINEERING, EVANSTON, IL 60208, USA

* Corresponding author: yeshin@kitech.re.kr



2. Experimental

Commercial A7075 aluminum alloy was machined into specimens suitable for BAF tests, and the detailed specimen geometry has been described in previous studies [6]. Severe plastic deformation was imposed through BAF processing for 4 passes under two different deformation conditions: room temperature and 300°C. The effective strain corresponding to the applied BAF passes was estimated based on previously reported strain accumulation during BAF processing [6]. After deformation, the microstructural characteristics of the processed specimens were examined using scanning electron microscopy equipped with energy-dispersive spectroscopy (SEM-EDS), with particular attention to compositional variations in the matrix region. In addition, electron backscatter diffraction (EBSD) analysis was performed to characterize deformation-induced microstructural features, including crystallographic orientation distributions and grain boundary characteristics. Fig. 1 illustrates the deformation distribution on the observed surface of the A7075 alloy after biaxial alternate forging. Based on the deformation map, the observation area was divided into regions with different deformation intensities. The central region, denoted as C, corresponds to the highly deformed zone, where the maximum strain accumulation is expected during BAF processing. In contrast, the regions marked as U represent the relatively low-deformation zones, where strain localization is limited. Microstructural and compositional analyses were conducted separately in these regions to

evaluate the effect of deformation intensity on microstructural evolution. It should be noted that the material used in this study was not subjected to prior aging treatment. Therefore, precipitation strengthening phases are not expected to be significantly developed prior to deformation. The selected U and C regions are considered representative of low- and high-deformation conditions, respectively, based on the strain distribution shown in Fig. 1, and were consistently identified across the samples.

3. Results and discussion

Fig. 2 shows SEM-BSE images of the A7075 alloy after four-pass BAF conducted at room temperature and 300°C. In both conditions, the overall distribution, morphology, and size of secondary-phase particles appear broadly similar, consisting of finely dispersed bright particles embedded in the aluminum matrix. No pronounced fragmentation, elongation, or dissolution of the secondary phases is observed as a function of deformation temperature at this magnification. In addition, macroscopic cracking or localized damage associated with severe deformation is not evident in either condition, indicating that the applied BAF process was successfully accommodated by the alloy. Although no significant differences were observed in the overall microstructural features or secondary-phase distributions between the two deformation conditions, matrix-level compositional analysis revealed a clear temperature-dependent variation. TABLE 1

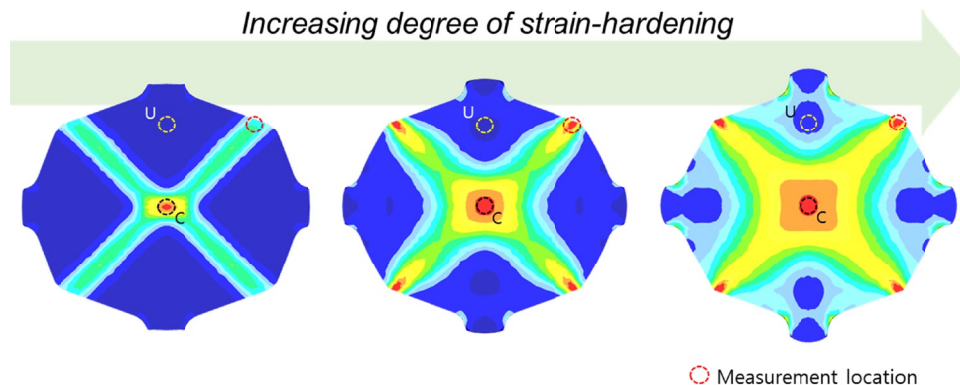


Fig. 1. Relative distribution of effective strain on the central cross-section of the workpiece depending on the degree of strain-hardening

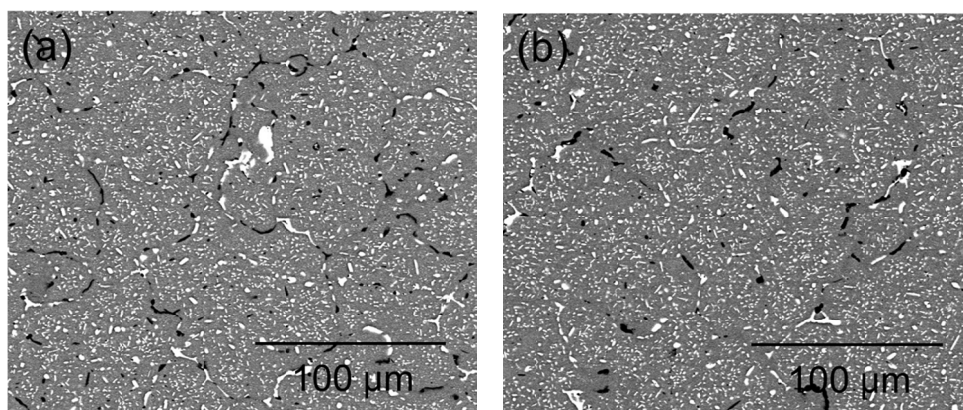


Fig. 2. SEM-BSE images of the cross-sectional surface of the A7075 alloy workpiece after four-pass BAF: (a) room temperature and (b) 300°C

summarizes the EDS results obtained from the matrix regions of the A7075 alloy after four-pass BAF at room temperature and 300°C. Compared to the room-temperature condition, the specimen deformed at 300°C exhibits a noticeable reduction in Zn content, decreasing from 5.03 to 3.85 mass%, accompanied by slight decreases in Mg and Cu contents. The reduction in Zn content in the matrix at 300°C suggests that enhanced solute redistribution may occur during high-temperature deformation. However, this interpretation should be considered with caution, as such compositional changes may also be influenced by increased atomic mobility, leading to solute partitioning toward existing coarse second-phase particles or local compositional heterogeneity, rather than the formation of new fine precipitates.

TABLE 1

Matrix composition of the A7075 alloy after four-pass BAF at room temperature and 300°C, determined by SEM-EDS analysis

Temp. (°C)	Analyzed composition (mass%)			
	Mg	Zn	Cu	Al
RT	2.86	5.03	1.88	Bal.
300	2.58	3.85	1.23	Bal.

Fig. 3 presents the EBSD analysis results of the A7075 alloy subjected to four-pass biaxial alternate forging at room temperature. Fig. 3(a) and (d) show the IQ maps of the low-deformation region (U region) and high-deformation region (C region), respectively. The IQ map of the U region exhibits relatively uniform contrast with localized variations, indicating limited strain accumulation without significant grain fragmentation. In contrast, the C region shows pronounced contrast reduction and band-like features, suggesting severe lattice distortion and in-

tense strain localization under repeated deformation. Representative shear and rolling texture components based on orientation distribution function (ODF) sections are shown in Fig. 3(b), (c) and (e), (f), respectively. In the U region, both shear and rolling texture components are weak and broadly distributed, indicating limited crystallographic reorientation under room-temperature deformation. In the C region, although the texture components become slightly more recognizable due to increased strain, the overall intensity remains low and the distribution remains diffuse. These results suggest that deformation at room temperature leads primarily to heterogeneous strain accumulation with limited development of well-defined textures.

Fig. 4 shows the EBSD analysis results of the A7075 alloy after four-pass biaxial alternate forging at 300°C. Fig. 4(a) presents the IQ map, which exhibits more uniform contrast compared to the room-temperature condition, indicating reduced lattice distortion due to enhanced recovery during deformation. The absence of pronounced band-like features suggests effective dislocation rearrangement at elevated temperature. The IPF map in Fig. 4(b) reveals a relatively homogeneous grain structure with reduced intragranular orientation gradients compared to the room-temperature condition. Although the overall grain size remains comparable, the lower internal misorientation indicates the formation of stabilized deformation substructures rather than heavily strained regions. Representative shear and rolling texture components are shown in Figs. 4(c) and 4(d). Compared to the room-temperature condition, the texture components appear more continuous, indicating that elevated temperature promotes crystallographic reorientation by enhancing dislocation mobility. However, the overall texture intensity remains moderate, suggesting that deformation at 300°C favors more uniform plastic flow accompanied by recovery rather than strong

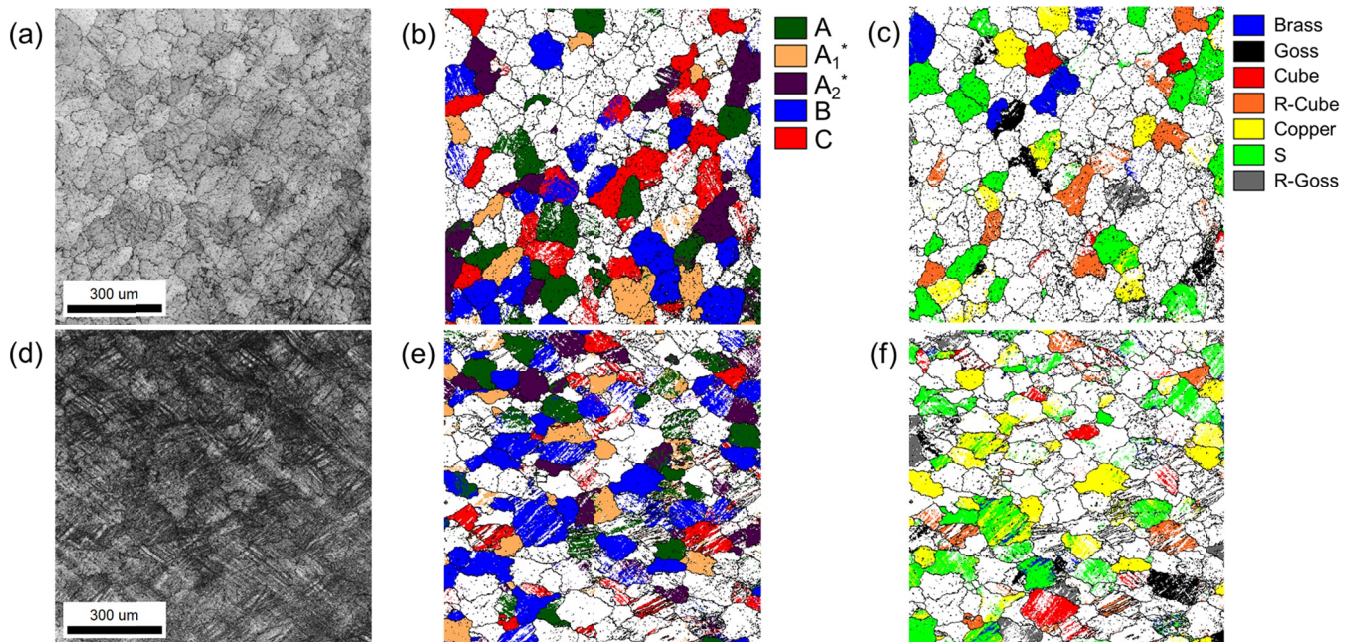


Fig. 3. EBSD analysis results of the A7075 alloy after four-pass biaxial alternate forging at room temperature: (a) IQ map of the low-deformation region (U), (b) representative shear texture component of the U region, (c) representative rolling texture component of the U region, (d) IQ map of the high-deformation region (C), (e) representative shear texture component of the C region, and (f) representative rolling texture component of the C region

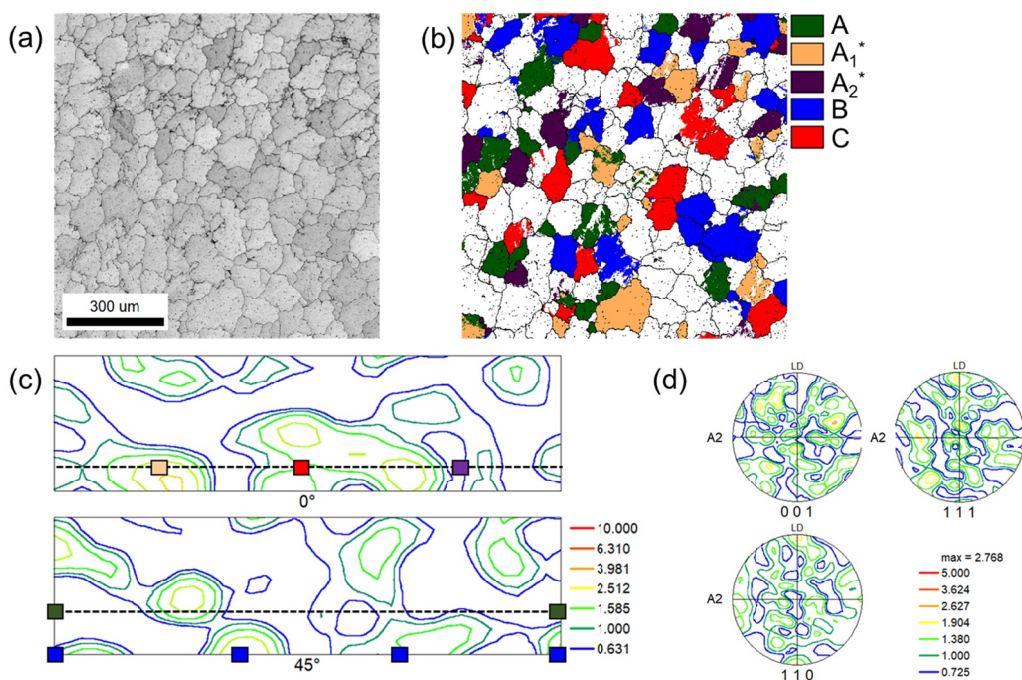


Fig. 4. EBSD analysis results of the A7075 alloy after four-pass biaxial alternate forging at 300°C: (a) IQ map, (b) map, (c) representative ODF section showing shear texture component, and (d) representative ODF section showing rolling texture component

texture sharpening. The reduced intragranular misorientation observed at 300°C can be attributed to recovery-assisted dislocation rearrangement facilitated by enhanced atomic mobility, rather than precipitation-related effects. Under this condition, the deformation behavior is more strongly governed by solute redistribution and recovery processes rather than precipitation evolution typically observed in aged A7075 alloys.

Overall, deformation at 300°C promotes a more homogeneous deformation mode through recovery-assisted dislocation rearrangement and enhanced solute mobility. This results in reduced lattice distortion and more stable texture evolution compared to room-temperature deformation. The temperature-dependent behavior of A7075 in the present study is therefore primarily governed by diffusion-assisted processes rather than precipitation kinetics.

4. Conclusions

The present study demonstrates that deformation temperature plays a critical role in governing the microstructural response of A7075 alloy during severe deformation by BAF. While the overall morphology and distribution of second-phase particles remained largely unchanged regardless of deformation temperature, clear differences were observed in matrix chemistry and deformation substructures. Deformation at 300°C led to a measurable decrease in Zn content within the matrix, implying enhanced solute redistribution during high-temperature processing. EBSD results revealed that RT deformation produced highly heterogeneous deformation structures with strong lattice distortion in high-strain regions, whereas deformation at 300°C promoted more uniform orientation distributions and reduced

internal misorientation, consistent with active recovery. Texture evolution under both conditions was characterized by moderate shear- and rolling-related components, with elevated temperature favoring more stabilized and continuous texture features rather than strong sharpening. Overall, the results indicate that high-temperature BAF enhances microstructural stability through recovery and solute redistribution, even when second-phase characteristics remain essentially unchanged.

Acknowledgments

This study has been conducted with the support of the National Research Foundation of Korea (NRF) grant funded by the Korea government (MSIT) (No. [RS-2024-00441999]).

REFERENCES

- [1] J.R. Davis (Ed.), *Aluminum and Aluminum Alloys*, ASM International, Materials Park, OH (1993).
- [2] I.J. Polmear, *Light Alloys: From Traditional Alloys to Nanocrystals*, 4th ed., Butterworth-Heinemann, Oxford (2006).
- [3] E.A. Starke, J.T. Staley, *Prog. Aerosp. Sci.* **32**, 131 (1996).
- [4] Y.C. Shin, S.H. Ha, A.W. Shah, *Arch. Metall. Mater.* **68** (2023).
- [5] Y.C. Shin, S.H. Ha, *Arch. Metall. Mater.* **69** (2024).
- [6] Y.C. Shin, S.H. Ha, B.H. Kim, Y.O. Yoon, S.H. Lim, H.J. Choi, S.K. Kim, S.K. Hyun, *J. Mater. Process. Technol.* **286**, 116822 (2020).
- [7] S.H. Ha, Y.C. Shin, *Materials* **17**, 968 (2024).